J Solid State Electrochem (2004) 8: 674–680
DOI 10.1007/s10008-004-0507-z

ORIGINAL PAPER

E. V. Tsipis · V. V. Kharton · I. A. Bashmakov
E. N. Naumovich · J. R. Frade

Cellulose-precursor synthesis of nanocrystalline $Ce_{0.8}Gd_{0.2}O_{2-\delta}$ for SOFC anodes

Received: 11 April 2003 / Accepted: 29 September 2003 / Published online: 11 March 2004

Abstract Developments of intermediate-temperature solid oxide fuel cells (IT SOFCs) require novel anode materials with a high electrochemical activity at 800–1070 K. The polarization of cermet anodes, made of nickel, ceria and yttria-stabilized zirconia (YSZ) and applied onto a YSZ solid electrolyte, can be significantly reduced by catalytically active ceria additions, the relative role of which increases with decreasing temperature. Further improvement is observed when using $Ce_{0.8}Gd_{0.2}O_{2-\delta}$(CGO) having a high oxygen ionic conductivity instead of undoped ceria, owing to enlargement of the electrochemical reaction zone. Nanocrystalline CGO powders with grain sizes of 8–35 nm were thus synthesized via the cellulose-precursor technique and introduced into Ni–CGO–YSZ cermets, and tested in contact with a $(La_{0.9}Sr_{0.1})_{0.98}Ga_{0.8}Mg_{0.2}O_{3-\delta}$(LSGM) electrolyte at 873–1073 K. The results showed that the anode performance can be enhanced by additional surface activation, in particular by impregnation with a Ce-containing solution, and also by incorporation of YSZ, which probably acts as a cermet-stabilizing component. The overpotential of the surface-modified Ni–CGO (25 wt%–75 wt%) anode in a 10% H_2/90% N_2 atmosphere was approximately 110 mV at 1073 K with a current density of 200 mA/cm^2.

Keywords Cellulose-precursor synthesis · Cermet · Electrode polarization · Nanocrystalline ceria · Solid oxide fuel cell anode

Presented at the OSSEP Workshop "Ionic and Mixed Conductors: Methods and Processes", Aveiro, Portugal, 10–12 April 2003

E. V. Tsipis (✉) · V. V. Kharton · J. R. Frade
Department of Ceramics and Glass Engineering,
CICECO, University of Aveiro,
3810-193 Aveiro, Portugal
E-mail: etsipis@cv.ua.pt
Tel.: +351-234-370263
Fax: +351-234-425300

V. V. Kharton · I. A. Bashmakov · E. N. Naumovich
Institute of Physicochemical Problems,
Belarus State University,
14 Leningradskaya Str.,
220050 Minsk, Belarus

Introduction

Decreasing the operating temperature of solid oxide fuel cells (SOFCs) down to 773–973 K, which is desirable due to important economical and technological advantages, requires optimization of the anode composition and microstructure in order to achieve sufficiently low overpotentials in the intermediate temperature range [1, 2, 3, 4]. One possible approach is to enhance the electrochemical activity of conventional anode cermets, consisting of metallic Ni and yttria-stabilized zirconia (YSZ), by the incorporation of catalytically active phases containing ceria [3, 4, 5, 6, 7, 8]. At the same time, the presence of YSZ may still be desirable in order to provide the necessary stability with respect to redox cycling and sintering. Owing to extensive volume changes resulting from oxygen partial pressure or current variations, large concentrations of ceria-based components in the cermets may lead to their instability [8]; on the other hand, stabilized zirconia possesses an essentially constant oxygen stoichiometry and, hence, volume under the anode operating conditions. The zirconia-based component may efficiently prevent sintering of nickel particles; for example, no sintering of 8% yttria-stabilized zirconia (Y8SZ) was observed in Ni–Y8SZ anodes after 4000 h at 1273 K [9].

An enhancement of the anode electrochemical activity could also be expected from the use of nanocrystalline ceria-containing powders, further sintering of which should be rather limited at intermediate temperatures. In addition to a greater surface area, decreasing the particle size down to the nano-scale should considerably affect both the transport and electrocatalytic properties, owing to a reduced defect formation energy and a high concentration of grain boundaries on the surface [10, 11, 12, 13]. As a particular result, nanocrystalline ceria exhibits

a substantially higher electronic conduction and faster oxygen exchange compared to materials with micron-scale grain sizes [10, 13].

The present work continues our studies of CeO_2-based materials for high-temperature electrochemical applications [14, 15, 16, 17] and is centered on the evaluation of anodes containing nanocrystalline $Ce_{0.8}Gd_{0.2}O_{2-\delta}$(CGO). Use of this phase, having a significant mixed ionic-electronic conductivity in reducing conditions [14], might be even advantageous with respect to undoped CeO_x, additions of which are known to drastically increase anode performance [7]. One particular goal included therefore an assessment of the roles of ionically conducting oxide components, such as CGO and YSZ, in the cermets.

Experimental

Nanocrystalline powders of single-phase $Ce_{0.8}Gd_{0.2}O_{2-\delta}$(CGO) and a two-phase NiO–CGO mixture, used for the fabrication of anode layers applied onto a $(La_{0.9}Sr_{0.1})_{0.98}Ga_{0.8}Mg_{0.2}O_{3-\delta}$(LSGM) solid electrolyte, were prepared by the cellulose-precursor method, earlier tested for synthesis of other mixed conductors [7, 18, 19]. This technique is based on the combustion of a structurally modified cellulose containing metal salts. For the synthesis, the starting cellulose fiber was reacted with a 65–70% solution of nitric acid, resulting in formation of the so-called Knecht compound, $(C_6H_{10}O_5{\cdot}HNO_3)_n$; the latter was then hydrolyzed in order to increase the sorption ability. The prepared structure-modified cellulose matrix was impregnated with aqueous solutions of the corresponding metal nitrates (Ce:Gd cation ratio of 8:2 or Ce:Gd:Ni cation ratio of 8:2:10); the impregnation ratio was 1.2–1.5 mL/g. Then the cellulose fibers were dried and ignited, forming oxide fibers retaining the precursor texture. In order to ensure complete firing of the carbon-containing residuum, the materials were annealed in air at 1173 K for 2 h. Formation of a single fluorite-type CGO phase or a two-phase CGO–NiO mixture was confirmed by X-ray diffraction (XRD) studies (Fig. 1). After annealing, the oxide fibers were either converted into nanocrystalline powders by light mechanical action, or directly applied onto dense LSGM ceramics and sintered; the nanostructured powders were mixed with other components of the anode cermets, screen printed onto LSGM and then annealed. Table 1 summarizes the anode compositions used in this work, and their preparation conditions. The anodes tested in contact with a 10% yttria-stabilized zirconia (Y10SZ) solid electrolyte were prepared as described elsewhere [7]. In all cases, the sheet density of the porous anode layers was 15 ± 3 mg/cm^2.

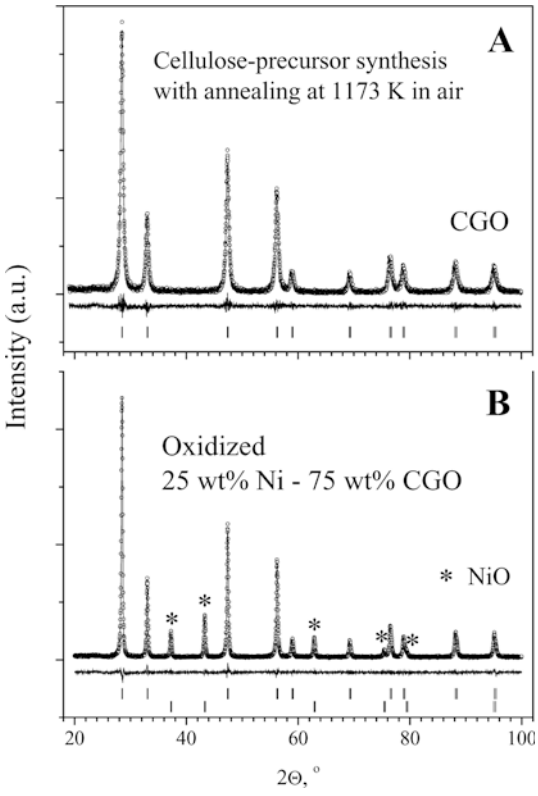

Fig. 1 Observed, calculated and difference XRD patterns for (**A**) $Ce_{0.8}Gd_{0.2}O_{2-\delta}$(CGO) and (**B**) 25 wt% NiO–75 wt% CGO mixture prepared via the cellulose-precursor technique and annealed in air at 1173 K

As-prepared powders and anode layers before and after the polarization measurements were characterized by XRD, transmission electron microscopy (TEM), electron diffraction and scanning electron microscopy (SEM) coupled with energy dispersive spectroscopy (EDS). The TEM/EDS and electron diffraction studies were performed using a Hitachi H-9000 instrument (300 kV). The cation composition of selected oxide fibers was verified by ion-coupled plasma (ICP) spectroscopic analysis. The experimental procedures and equipment used for the characterization have been reported elsewhere ([7, 14, 15, 16, 17, 18, 19] and references cited therein). Structural parameters were refined from XRD data using the Fullprof program [20]; examples of the final Rietveld plots are given in Fig. 1.

Table 1 Preparation conditions for ceria-containing SOFC anodes

Anode composition[a]	Solid electrolyte	Preparation conditions
Ni–Y8SZ–CGO 50–30–20 wt% (42–37–21 vol%)	LSGM	Decomposition of $Ni(NO_3)_2{\cdot}6H_2O$; cellulose-precursor synthesis of CGOMixing and grinding of Ni, CGO and commercial Y8SZ Screen printingAnnealing in air at 1523 K for 2 h Reduction at 1073–1123 K in 10% H_2/90% N_2 mixture
Ni–CGO 25–75 wt% (21–79 vol%)	LSGM	Cellulose-precursor synthesis of NiO–CGO mixture Screen printingFiring in air at 1573 K for 2 h Reduction at 1073–1123 K in 10% H_2/90% N_2 mixture
Ni–Y10SZ–$CeO_{2-\delta}$ 54–(46−x)–x wt% (44–(56−x)–x vol%) andNi–Y10SZ–CGO 54–17–29 wt% (47–22–31 vol%)	Y10SZ	Decomposition of $Ni(NO_3)_2{\cdot}6H_2O$; mixing with commercial powders and ball millingScreen printingFiring at 1373 K in air Reduction at 1173–1273 K in wet 10% H_2/90% N_2 mixture

[a]The volume percentage was estimated from the weight percentage and theoretical densities calculated from XRD data at room temperature in air, neglecting oxygen stoichiometry variations and counting solid phases only

The anodic overpotential dependences on the current density were studied by a three-electrode technique in cells with porous Pt counter and reference electrodes (CE and RE, respectively); the cell geometry was chosen according to published details [21, 22]. The working electrode (WE) and CE were symmetrically deposited onto different sides of solid electrolyte disks; the diameter of these electrodes was 6 mm. The distance between the WE and RE (diameter 1 mm) was 5–6 mm. The polarization measurements were performed using an AUTOLAB PGSTAT20 instrument at 873–1223 K in flowing dry 10% H_2/90% N_2 or 3% H_2O/10% H_2/87% N_2 gas mixtures; the oxygen partial pressure, $p(O_2)$, was independently measured by an oxygen sensor. The overpotential (η) was calculated as $\eta = U - I \times R$, where U is the potential difference between the WE and RE, I is the current between the WE and CE, and $I \times R$is the ohmic contribution to the total potential drop. The values of the corresponding ohmic resistance, R, were obtained from the impedance spectra, an example of which is shown in Fig. 2. The steady-state anodic current density and overpotential varied in the ranges 0–300 mA/cm^2 and 0–460 mV, respectively; the time necessary to achieve steady-state conditions was 1–3 h. The reproducibility of the results was separately checked after each measurement cycle; one representative example is given as an inset in Fig. 2. For different anodes of identical composition, the standard deviation of the overpotential values at a fixed current density was about 12–15% at 1073–1223 K; for one sample after approximately 200 h of testing, the maximum deviation from the initial overpotential values was lower than 5–7%. After the electrochemical measurements, selected anode layers were surface modified by impregnation with saturated $Ce(NO_3)_3 \cdot 6H_2O$ solution in ethanol, followed by annealing at 1073–1273 K; then the overpotential–current dependences were re-measured.

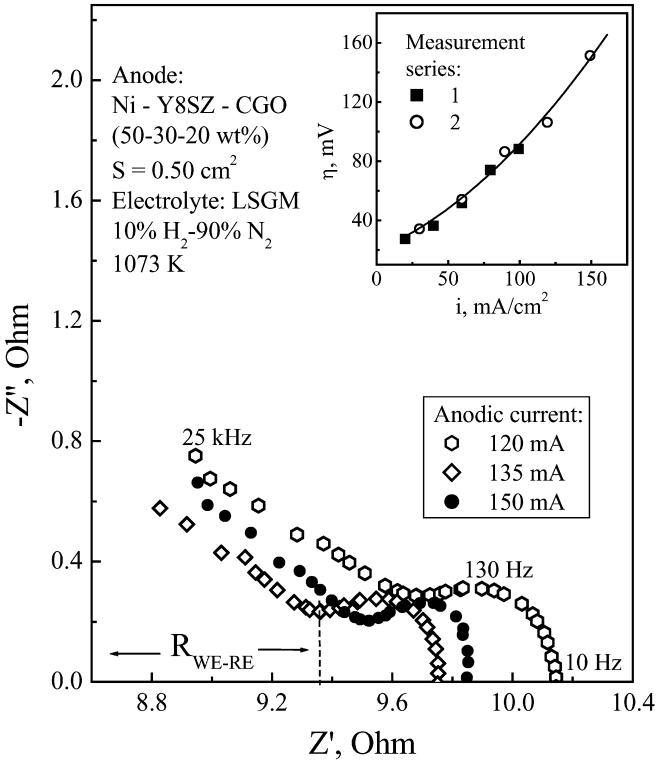

Fig. 2 Typical impedance spectra for a 50 wt% Ni–30 wt% Y8SZ–20 wt% CGO cermet anode obtained in the course of polarization measurements at 1073 K. The *inset* shows the results of one reproducibility test of the overpotential versus current density dependence

Results and discussion

Behavior of CeO_2-containing anodes in contact with YSZ

Figure 3 shows the overpotential dependence on the ceria content in anode layers at a fixed current density of 100 mA/cm^2; the general composition of the anodes applied onto the Y10SZ electrolyte is 54 wt% Ni–(46−x) wt% Y10SZ–x wt% $CeO_{2-\delta}$ ($x = 0$–40). When the temperature is high, the anode performance is moderately influenced by the ceria additive. For example, at 1223 K, adding 10–20 wt% of ceria leads to a decreasing overpotential from approximately 40 mV down to 25 mV; further additions result in a worse performance. This behavior seems in agreement with the literature data [3, 4, 5, 7, 23, 24] and may be explained by an enhancement of the anode electrocatalytic activity due to the incorporation of $CeO_{2-\delta}$, which may be, however, quite passivated after thermal treatment at 1273–1373 K (Table 1). Although a significant oxygen nonstoichiometry of $CeO_{2-\delta}$ in reducing atmospheres [23] makes it possible to expect substantial ionic transport, the conductivity of the YSZ electrolyte at 1173–1223 K is also high [24]; no essential improvement due to ionic conduction in ceria could be expected under these conditions. For instance, a parallel anodic reaction path at 1273 K, with H_2 oxidation occurring at the Y8SZ surface, has been suggested [25]. The optimum anode performance is hence obtained when combining two ionically conductive components, catalytically active $CeO_{2-\delta}$ and cermet-stabilizing YSZ. When the temperature decreases, a pronounced shift of the overpotential minimum towards a higher Ce concentrations is observed, indicating a greater role for the electrocatalytic

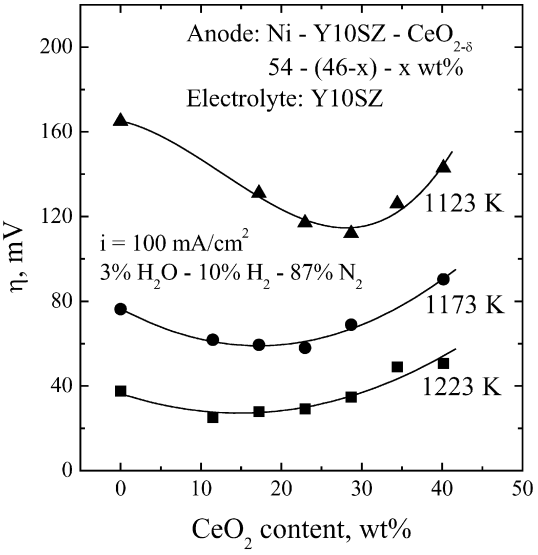

Fig. 3 Anodic overpotentials of Ni–YSZ–$CeO_{2-\delta}$ cermet layers in contact with a Y10SZ solid electrolyte at 100 mA/cm^2

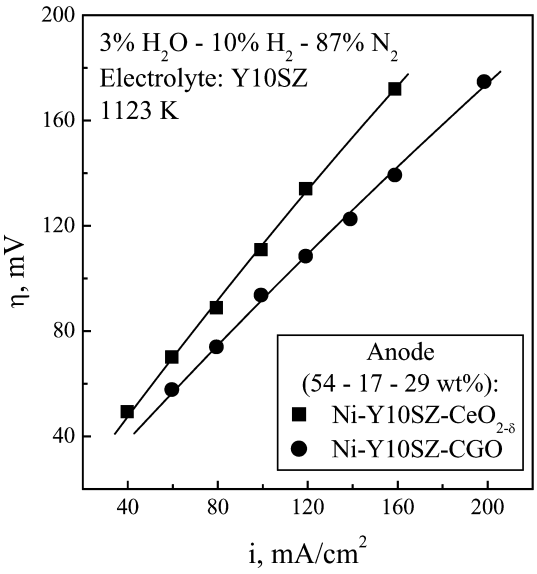

Fig. 4 Anodic current density dependence of the overpotential for two cermet compositions containing 29 wt% of $CeO_{2-\delta}$ or CGO at 1123 K

activity of the anode layers (Fig. 3). Nonetheless, the minimum overpotential is still achieved if combining yttria-stabilized zirconia and ceria in the cermets.

In order to assess the role of the oxygen ionic conductivity of the anode components, Fig. 4 compares the overpotential versus current dependences for two cermet compositions containing Ni, Y10SZ and $CeO_{2-\delta}$ or CGO; the microstructure of both cermets was similar. At 1123 K, the polarization of the CGO-containing anode is 15–25% lower with respect to the layer comprising the undoped ceria. At higher temperatures this difference was found to become rather negligible; in fact, the performance of the latter cermet composition at 1223 K was even slightly higher. This suggests that the effect of ionic transport in cermet components, resulting in an enlargement of the electrochemical reaction zone, becomes more important when the temperature decreases, in agreement with the literature [3, 4].

Summarizing these results, one can conclude that the use of CGO in the intermediate temperature range is preferable compared to undoped ceria. Although the ionic conductivity of YSZ at temperatures below 1123 K is insufficient for a high anode performance, incorporation of YSZ in the cermet compositions might still be important to provide the necessary stability of the anode layers.

Cellulose-precursor synthesis of anode components

SEM studies of oxide fibers made of CGO (Fig. 5A) and NiO–CGO (Fig. 6A) showed that the precursor texture is retained after combustion; the fibres have a highly porous tubular-like microstructure (Fig. 5B). Such a feature may be advantageous for the preparation of anodes with regular microstructures, which can be further optimized by taking the electrode reaction mechanisms into account. In particular, by varying the type of cellulose precursor, this technique makes it possible to achieve the necessary relationships between the size and

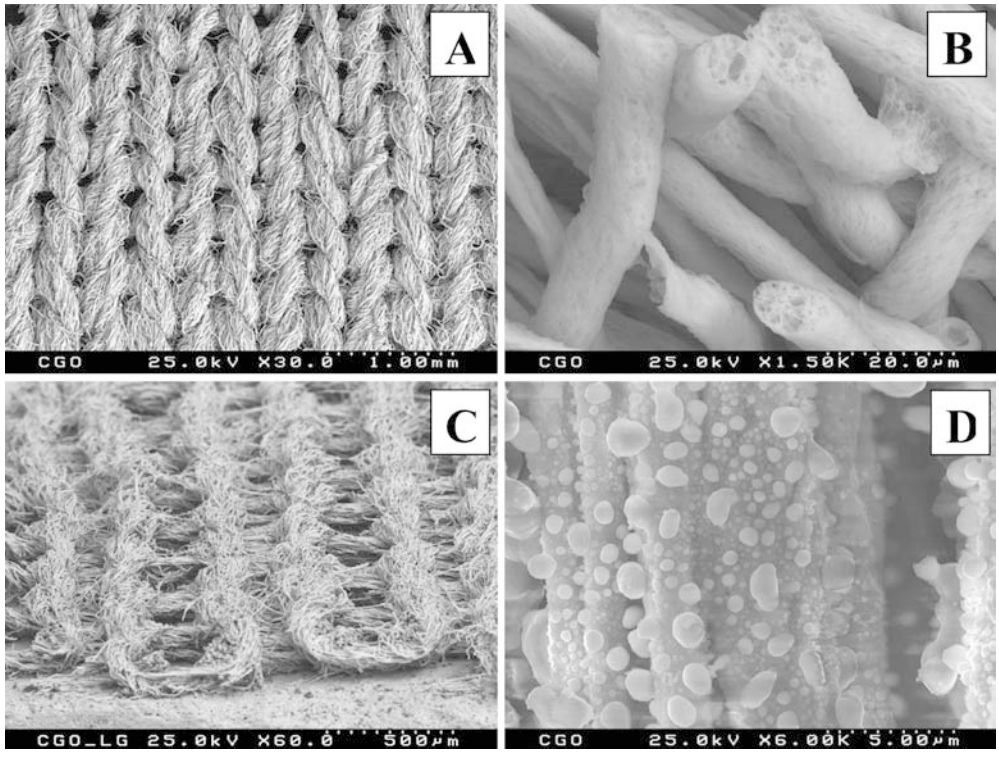

Fig. 5 SEM micrographs of CGO synthesized via the cellulose-precursor technique: (**A**, **B**) after synthesis and annealing in air at 1173 K; (**C**) applied onto LSGM substrate and annealed in air at 1573 K (cross-section view); (**D**) applied onto LSGM with subsequent deposition of metallic Ni (50 wt%) by impregnation with an aqueous $Ni(NO_3)_2{\cdot}6H_2O$ solution and reduction at 1273 K in flowing 10% H_2/90% N_2

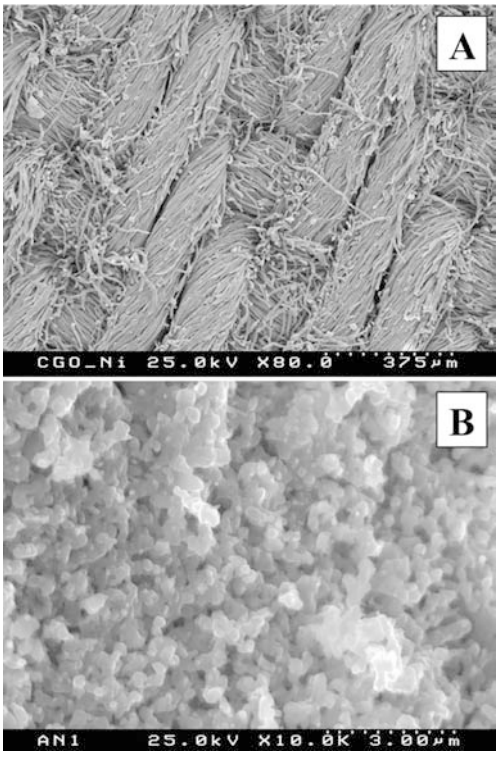

Fig. 6 SEM micrographs of: (**A**) NiO–CGO fiber prepared by the cellulose-precursor technique and annealed in air at 1173 K; (**B**) 25 wt% Ni–75 wt% CGO anode obtained from the fibers after surface modification via impregnation with Ce-containing solution, reduction and testing during ca. 340 h

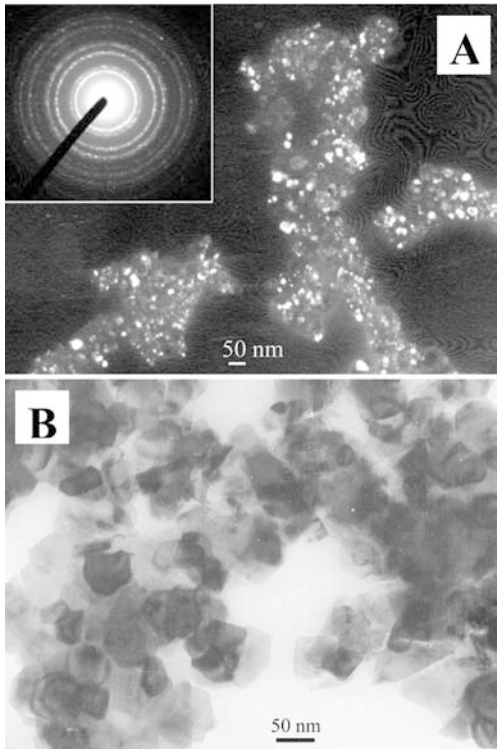

Fig. 7 (**A**) Dark-field TEM image and electron diffraction pattern of CGO and (**B**) bright-field image of a NiO–CGO mixture, both prepared using the cellulose-precursor technique and annealed in air at 1173 K

distribution of the pores, the specific surface area, the distribution of the electronically conducting phase, the triple-phase boundary length and other factors determining anode performance. Furthermore, sintering of the highly porous oxide fibers onto the solid electrolyte substrate can be used to form an ion-conducting ceramic matrix stabilizing metallic Ni with respect to sintering and redox cycling.

TEM inspection revealed that CGO particles constituting oxide fibers are nanocrystalline; their size varies in the range 8–35 nm (Fig. 7A). The crystallization of the CGO phase was verified by electron diffraction studies; one example of the electron diffraction pattern is presented as the inset in Fig. 7A. For NiO–CGO fibers, TEM confirmed that the phase distribution is quite uniform, whilst the particle size is larger, up to 80 nm (Fig. 7B). The unit cell parameters of fluorite-type CGO phase, calculated from XRD data, were almost equal for all synthesized materials: 0.54250 ± 0.00005 nm. This suggests, in particular, that the interaction of CGO and NiO in the two-phase mixture is negligible.

Owing to the potential advantages of anode microstructure control by the cellulose-precursor selection, direct application of oxide or cermet fibers onto solid electrolyte ceramics might be of a considerable interest. A series of electrode layers was thus prepared by applying CGO fibers onto LSGM, followed by annealing, impregnation with Ni-containing solutions and reduction. As an example, Fig. 5C presents the cross-section SEM micrograph of one layer made of a CGO fiber after annealing at 1573 K for 2 h. The fiber forms a porous ceramic matrix with relatively good adhesion to the electrolyte and a regular microstructure suitable for metal incorporation. After impregnation with an aqueous solution of $Ni(NO_3)_2 \cdot 6H_2O$ and firing at 1273 K in a flow of a 10% H_2/90% N_2 mixture for 0.25 h, metallic nickel is uniformly distributed in the CGO fibres in the layer containing 50 wt% Ni and 50 wt% CGO (Fig. 5D). At the same time, the stability of such Ni–CGO anodes in the course of redox cycling was found insufficient, most probably due to volume changes. Further developments necessary to prepare stable anode layers, by directly applying ceramic fibers onto the electrolyte ceramics, are now in progress. In this work, therefore, the main emphasis is given to the CGO-containing cermets, where the nanocrystalline powders synthesized using the cellulose-precursor technique were mixed with other components, as listed in Table 1.

CGO-containing anodes in contact with LSGM

Figure 8 compares overpotential versus current dependences of Ni–CGO and Ni–CGO–Y8SZ anodes, deposited onto LSGM, at 1073 K; the compositions and fabrication conditions are given in Table 1. The

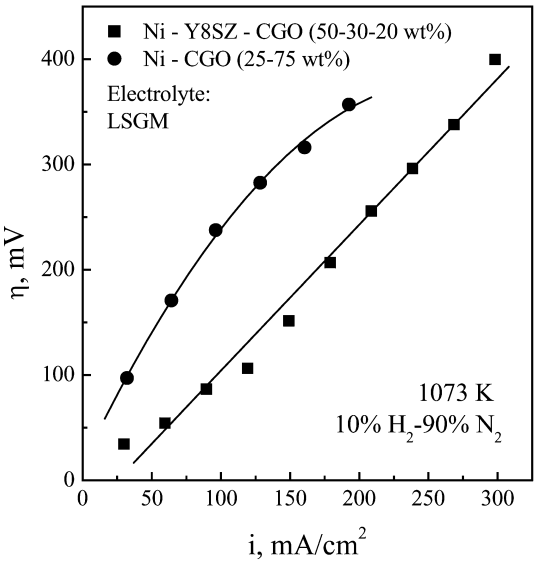

Fig. 8 Overpotential versus anodic current density dependences of the CGO-containing anodes in contact with LSGM electrolyte at 1073 K

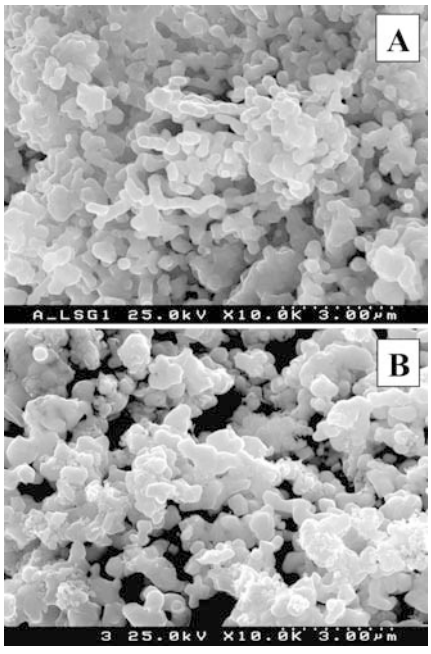

Fig. 9 SEM micrographs of 50 wt% Ni–30 wt% Y8SZ–20 wt% CGO anode layers (**A**) before and (**B**) after electrochemical measurements during ca. 200 h

electrochemical performance of the Ni–Y8SZ–CGO cermet in contact with the LSGM electrolyte is higher than that of similar compositions applied onto YSZ (Fig. 3). Most likely, this is associated with the higher activity of nano-sized CGO particles in the former case, and also with the influence of the ionic conductivity of the solid electrolyte on the anode exchange currents, which becomes significant at intermediate temperatures [4]. At 1073 K and a fixed current density of 200 mA/cm^2, the overpotential of the Ni–Y8SZ–CGO anode is lower than 245 mV (Fig. 8). SEM micrographs of this layer, as-prepared and after testing for approximately 200 h, are presented in Fig. 9A and Fig. 9B, respectively. Both microstructures are quite homogeneous; the grain agglomeration that occurs at elevated temperatures is insignificant.

The YSZ-containing anode exhibits a higher electrochemical activity compared to Ni–CGO (Fig. 8), which could be attributed either to a stabilizing influence of zirconia or to a higher Ni content in the Ni–CGO–Y8SZ cermet. However, the data on the surface-activated Ni–CGO layer (Fig. 10A) indicate that the performance can be improved by further ceria additions, decreasing the Ni concentration down to 21 vol%. Therefore, the total Ni concentration above the percolation limit cannot be considered as a performance-determining factor. Since the ionic conductivity of YSZ at 1073 K is considerably lower than that of CGO, one may suggest that the major role of YSZ refers to mechanical stabilization of the cermet, in particular with respect to re-oxidation at high anodic currents. This well corresponds with the data on Ni–Y10SZ–$CeO_{2-\delta}$ layers in contact with a YSZ solid electrolyte (Fig. 3).

Another necessary comment is that although the ionic conductivity of CGO is higher than that of undoped ceria, incorporating $CeO_{2-\delta}$ via impregnation with Ce-containing solutions substantially increases the electrochemical activity (Fig. 10A). After the surface modification, the overpotential at 1073 K and 100–200 mA/cm^2 decreased 3–4 times. Such a behavior is related, first of all, to increasing catalytic activity of the anode layer due to incorporation of fine ceria particles formed after thermal decomposition of cerium nitrate. At the same time, the anode performance enhancement may also be contributed by improved electrical contacts between the particles, resulting from the significant electronic conductivity of ceria in reducing atmospheres [23]. Indeed, the microstructure of surface-modified Ni–CGO anodes (Fig. 6B) is less porous and more uniform compared to non-activated layers (e.g. Fig. 9).

Finally, the electrochemical activity of the surface-activated Ni–CGO cermet at 1073 K is relatively high; for example, the overpotential at 200 mA/cm^2 is about 110 mV. Decreasing the temperature below 973 K leads, however, to a rather poor performance (Fig. 10B). This makes it necessary to further optimize the anode composition and microstructure. Promising approaches include, in particular, the incorporation of nanocrystalline YSZ into CGO fibers with subsequent applying on solid electrolyte ceramics, use of higher Ni concentrations, modification of the electrolyte surface prior to anode deposition, and also doping of CGO in order to increase the n-type electronic transport.

Conclusions

The results on the anodic polarization of Ni–YSZ–CGO ($CeO_{2-\delta}$) cermet layers in contact with a YSZ solid

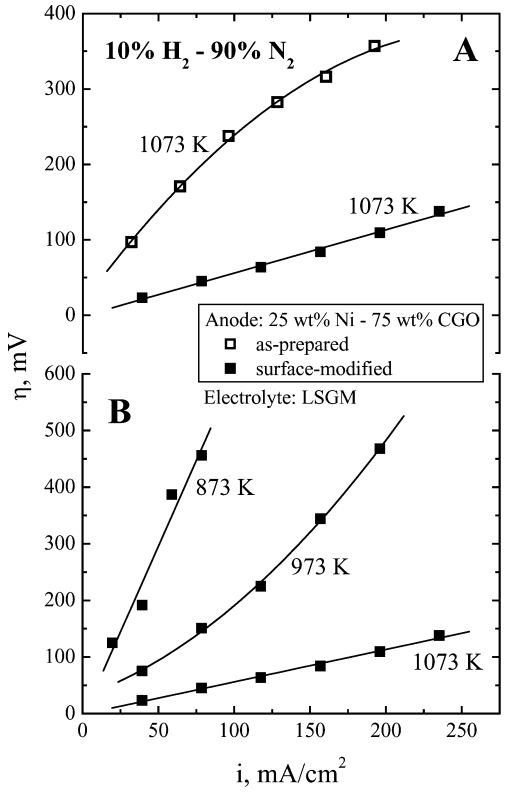

Fig. 10 Overpotential versus current density dependences of 25 wt% Ni–75 wt% CGO electrode in contact with LSGM solid electrolyte: (**A**) comparison of as-prepared and surface-modified anodes at 1073 K; (**B**) performance of surface-activated layer at 873–1073 K

electrolyte show that the anode performance at 1123–1223 K can be significantly increased by ceria-based additions. Owing to an enlargement of the electrochemical reaction zone resulting from the higher ionic conductivity of CGO compared to undoped ceria, the use of CGO provides higher electrochemical activity. Although the role of catalytically active ceria additions increases when the temperature decreases, the optimum performance is achieved if combining ceria with YSZ, which probably stabilizes cermets with respect to re-oxidation. Since an additional improvement could be expected from the use of nano-structured CGO, nanocrystalline powders of CGO (grain size 8–35 nm) and a NiO–CGO mixture (20–80 nm) were prepared using the cellulose-precursor technique. This method makes it possible, in particular, to fabricate electrode layers with regular microstructures and to stabilize metal components of the cermets by dispersing in a highly porous oxide matrix. Testing of Ni–CGO–YSZ anodes, comprising nanocrystalline Ce-containing powders and applied onto a LSGM electrolyte, demonstrated a relatively high activity, which can be further improved by surface modification via the impregnation with Ce-containing solutions. The presence of YSZ in the anodes seems desirable even at intermediate temperatures (873–1073 K). The overpotential of the surface-modified anode, containing 25 wt% Ni and 75 wt% CGO, was approximately 110 mV at 1073 K and a current density of 200 mA/cm^{2}in a flowing 10% H_2/90% N_2mixture.

Acknowledgements This work was partially supported by the FCT, Portugal (projects POCTI/CTM/3938/2001 and BD/6827/2001), by the NATO Science for Peace program (project 978002), and by the Belarus Ministry of Education. Experimental assistance of L.V. Solov'eva, A.A. Yaremchenko and N.P. Vyshatko is gratefully acknowledged.

References

1. Yamamoto O (2000) Electrochim Acta 45:2423
2. Huijsmans JPP (2001) Curr Opin Solid State Mater Sci 5:317
3. Ishihara T, Shibayama T, Nishiguchi H, Takita Y (2000) Solid State Ionics 132:209
4. Watanabe M, Uchida H, Yoshida M (1997) J Electrochem Soc 144:1739
5. Huang K, Heng M, Goodenough JB (1997) J Electrochem Soc 144:3620
6. Huijsmans JPP, Berkel FPF, Christie GM (1998) J Power Sources 71:107
7. Kharton VV, Naumovich EN, Tikhonovich VN, Bashmakov IA, Boginsky LS, Kovalevsky AV (1999) J Power Sources 77:242
8. Marina OA, Bagger C, Primdahl S, Mogensen M (1999) Solid State Ionics 123:199
9. Simwonis D, Tietz F, Stöver D (2000) Solid State Ionics 132:241
10. Tuller HL (2000) Solid State Ionics 131:143
11. Tschope A (2001) Solid State Ionics 139:267
12. Kharton VV, Marques FMB (2002) Curr Opin Solid State Mater Sci 6:261
13. Christie GM, van Berkel FPF (1996) Solid State Ionics 83:17
14. Kharton VV, Figueiredo FM, Navarro L, Naumovich EN, Kovalevsky AV, Yaremchenko AA, Viskup AP, Carneiro A, Marques FMB, Frade JR (2001) J Mater Sci 36:1105
15. Kharton VV, Viskup AP, Figueiredo FM, Naumovich EN, Yaremchenko AA, Marques FMB (2001) Electrochim Acta 46:2879
16. Fagg DP, Abrantes JCC, Perez-Coll D, Nunez P, Kharton VV, Frade JR (2003) Electrochim Acta 48:1023
17. Kharton VV, Viskup AP, Figueiredo FM, Naumovich EN, Shaulo AL, Marques FMB (2002) Mater Lett 53:160
18. Kharton VV, Tikhonovich VN, Shuangbao Li, Naumovich EN, Kovalevsky AV, Viskup AP, Bashmakov IA, Yaremchenko AA (1998) J Electrochem Soc 145:1363
19. Kharton VV, Figueiredo FM, Kovalevsky AV, Viskup AP, Naumovich EN, Yaremchenko AA, Bashmakov IA, Marques FMB (2001) J Eur Ceram Soc 21:2301
20. Rodriguez-Carvajal J (1993) Physica B 192:55
21. Mizusaki J, Tagawa H (1994) J Electrochem Soc 141:1674
22. Figueiredo FM, Frade J, Marques FMB (1999) Bol Soc Esp Ceram Vidrio 38:639
23. Mogensen M, Sammes NM, Tompsett GA (2000) Solid State Ionics 129:63
24. Kharton VV, Naumovich EN, Vecher AA (1999) J Solid State Electrochem 3:61
25. Brown M, Primdahl S, Mogensen M (2000) J Electrochem Soc 147:475